High-Mach-Number Turbulence Modeling using Machine Learning and Direct Numerical Simulation Database

Junji Huang* and Lian Duan†

Missouri University of Science and Technology, Rolla, MO 65409

Jianxun Wang‡ , Rui Sun‡ and Heng Xiao§

Virginia Tech, Blacksburg, Virginia, VA 24061

In this paper, a physics-informed machine learning approach is applied to improve the accuracy of the Reynolds stresses modeled by Reynolds-averaged Navier-Stokes (RANS) for high-speed flat-plate turbulent boundary layers using an existing DNS database. In the machine-learning technique, the DNS dataset of a Mach 2.5 adiabatic turbulent boundary layer is used as the training flow to construct the invariant basis for learning the functional form of the discrepancy in RANS modeled Reynolds stresses. The functional thus constructed is in turn used to correct the RANS prediction of Reynolds stresses for turbulent boundary layers under two cold-wall hypersonic conditions with nominal freestream Mach numbers of 6 and 8. The study shows that the RANS-modeled Reynolds normal stresses, the turbulent kinetic energy, and the Reynolds-stress anisotropy can be significantly improved using the machine-learning technique. Such a study lays the foundation towards better physics-based turbulence modeling for high-Mach-number turbulent flows.

Nomenclature

C_p	heat capacity at constant pressure, J/(K·kg)
C_v	heat capacity at constant volume, J/(K·kg)
H	shape factor, $H = \delta^*/\theta$, dimensionless
M	Mach number, dimensionless
Pr	Prandtl number, $Pr = 0.71$, dimensionless
R	ideal gas constant, $R = 287$, J/(K·kg), or radius of the axisymmetric nozzle, m
Re_θ	Reynolds number based on momentum thickness and freestream viscosity, $Re_\theta \equiv \frac{\rho_\infty U_\infty \theta}{\mu_\infty}$, dimensionless
Re_{δ_2}	Reynolds number based on momentum thickness and wall viscosity, $Re_{\delta_2} \equiv \frac{\rho_\infty U_\infty \theta}{\mu_w}$, dimensionless
Re_τ	Reynolds number based on shear velocity and wall viscosity, $Re_\tau \equiv \frac{\rho_w u_\tau \delta}{\mu_w}$, dimensionless
rms	root mean square
T	temperature, K
T_r	recovery temperature, $T_r = T_\infty(1 + 0.9 * \frac{\gamma-1}{2} M_\infty^2)$, K
U_∞	freestream velocity, m/s
a	speed of sound, m/s
p	pressure, Pa
q	dynamic pressure, Pa
r	radial coordinate
u	streamwise velocity, m/s

*Graduate Student, Student Member, AIAA

†Assistant Professor, Senior Member, AIAA

‡Graduate Student

§Assistant Professor

u_τ friction velocity, m/s
v wall-normal velocity, m/s
w spanwise velocity, m/s
x streamwise direction of the right-hand Cartesian coordinate
y wall-normal direction of the right-hand Cartesian coordinate
z spanwise direction of the right-hand Cartesian coordinate
z_τ viscous length, $z_\tau = \nu_w/u_\tau$, m
γ specific heat ratio, $\gamma = C_p/C_v$, dimensionless
δ boundary layer thickness, m
δ^* displacement thickness, m
κ thermal conductivity, $\kappa = \mu C_p/Pr$, W/(m·K)
θ momentum thickness, m
μ dynamic viscosity, $\mu = 1.458 \times 10^{-6} \frac{T^{3/2}}{T+110.4}$, kg/(m·s)
ν kinematic viscosity, $\nu = \mu/\rho$, m^2·s
ρ density, kg/m^3
ω frequency, rad/s

Subscripts

i inflow station for the domain of direct numerical simulations
rms root mean square
w wall variables
∞ freestream variables
t stagnation quantities

Superscripts

$+$ inner wall units
$\overline{(\cdot)}$ averaged variables
$(\cdot)'$ perturbation from averaged variable

I. Introduction

The information of the full Reynolds-stress tensor of a high-speed turbulent boundary layer is of theoretical and practical importance. Understanding the physics of the Reynolds stress and its dependence on boundary-layer parameters is critical for theoretical development of advanced compressibility corrections for Reynolds-Averaged Navier-Stokes (RANS) models.[1] The information is also useful for imposing the inflow boundary condition for high-fidelity simulations like direct numerical simulations (DNS) and large-eddy simulations (LES) if a synthetic turbulence-generation technique is used.[2] So far, there is only limited data for turbulent boundary layers in the high-Mach-number regime. Most of the experimental measurements are limited to basic turbulence quantities, such as the skin friction and Stanton number, the mean and root mean square (r.m.s.) fluctuations of velocity and temperature.[3] Existing DNS or LES studies are limited to low Reynolds numbers. As a result, the information of the full Reynolds-stress tensor in the high-Mach-number and high-Reynolds-number regimes is largely unknown.

RANS turbulence modeling offers a potential way for exacting information of Reynolds stresses. In RANS, the turbulence stresses can be derived, for instance, using the mean rate-of-strain tensor and the eddy viscosity from the turbulence models. Although large model-form uncertainties are known to exist in standard RANS models for Reynolds stress closure,[4] the accuracy and predictability of the RANS models can be improved by data-driven turbulence modeling using existing data (e.g., from DNS simulation or experiment). So far , a number of data-driven techniques have been proposed to assist the standard RANS modeling. For example, Dow and Wang[5] used DNS data to infer and correct the full-field discrepancy in the turbulent viscosity and applied it for a range of channel flows. Parish et al.[6] also tried to improve the RANS model by adding a full-field discrepancy function into the production term of the turbulence transport equation. As far as the prediction of Reynolds stresses are concerned, Xiao et al.[7] proposed a model-form uncertainty reduction framework by inferring the discrepancy of Reynolds stress based on sparse data of velocities. Ling et al.[8] used Random Forests classifier to predict when RANS assumptions would fail. Wang et al.[9] recently proposed a physics-informed, machine-learning (ML) approach to predict the discrepancy of RANS modeled Reynolds stress based on a group of training flows with data. Since the functional form of Reynolds stress discrepancy is learned in the mean flow feature space, it can be extrapolated to different

flows (at different Reynolds numbers or/and in modified geometries) without data. The effectiveness of the physics-informed ML approach for improving the prediction of Reynolds stress tensor based on RANS predicted mean flow fields has been demonstrated in multiple low-speed flows, including scenarios where the training flow has the same geometry as the prediction flow but is different in Reynolds numbers and scenarios where the training flow differs from the prediction flow not only in Reynolds numbers but also in geometry. The performance of the ML approach for high-speed flows has not been fully studied yet.

The primary objective of the present paper is to leverage an existing DNS database of high-speed flat-plate turbulent boundary layers and apply the physics-informed ML approach by Wang et al.[9] to evaluate the prediction of Reynolds stresses for high-Mach-number boundary-layer flows.

The paper is structured as follows. The methodology of ML approach is given in Section II, including a brief description of the DNS database to be used (Section A), the simulation details of the baseline RANS (Section B), and the detailed procedures of the ML approach (Section C). Results of applying the physics-informed ML approach for predictive turbulence modeling are shown in Section III. Summaries are given in Section IV.

II. Methodology

A. DNS Database of High-Speed Turbulent Boundary Layers

Relevant flow conditions of the DNS database that is utilized for the current analysis are summarized in Table 1, which provides the boundary-layer parameters at a selected location where the turbulence statistics are gathered. The database includes DNS of spatially-developing turbulent boundary layers over a wide range of freestream Mach numbers ($M_\infty = 2.5 - 7.9$). All the DNS cases have a similar Karman number of $Re_\tau \approx 400$. The details of the DNS database, including the numerical methodology and boundary conditions are described in multiple previous publications.[10–13]

Figures 1 shows the general computational setup for Case M6Tw076. The computational setup of the other cases parallels that of Case M6Tw076. For all cases, a long streamwise domain length with a large rescaling length ($> 50\delta_i$) for inflow turbulence generation is used to minimize any artificial effects of the rescaling procedure and to increase the streamwise extent and the Reynolds-number range of the DNS. Table 2 summarizes the domain sizes and grid resolutions for DNS cases. The DNS dataset will be used either as the training data in the physics-informed ML technique or as the validation data for testing the prediction of the ML technique.

Table 1. Boundary layer properties at the station selected for the analysis for various DNS cases.

Case	M_∞	T_w/T_r	Re_θ	Re_τ	Re_{δ_2}	$\theta(mm)$	H	$\delta(mm)$	$z_\tau(\mu m)$	$u_\tau(m/s)$
M25	2.5	1.0	2268.8	380.0	1326.1	0.47	2.6	5.5	14.5	42.1
M6Tw076	5.86	0.76	9655.5	436.3	1880.2	0.93	13.5	23.0	52.6	45.0
M8Tw053	7.87	0.53	8445.2	380.2	1607.0	0.87	19.1	26.3	69.0	53.3

Table 2. Grid resolutions and domain sizes for direct numerical simulations. L_x, L_y and L_z are the domain size in the streamwise, wall-normal, and spanwise directions, respectively. Δx^+ and Δz^+ are the uniform grid spacing in the streamwise and spanwise directions, respectively; Δy^+_{min} and Δy^+_{max} are the minimum and maximum wall-normal grid spacing. The grid resolutions are normalized by the viscous length at the location where the turbulence statistics are gathered.

Case	$N_x \times N_y \times N_z$	L_x/δ_i	L_y/δ_i	L_z/δ_i	Δx^+	Δz^+	Δy^+_{min}	Δy^+_{max}
M25	$1760 \times 400 \times 800$	57.3	41.0	15.6	9.0	5.4	0.6	9.0
M6Tw076	$1920 \times 500 \times 320$	74.4	39.7	6.3	9.6	5.1	0.52	5.32
M8Tw053	$3000 \times 500 \times 320$	64.1	32.4	5.5	5.0	4.0	0.37	3.84

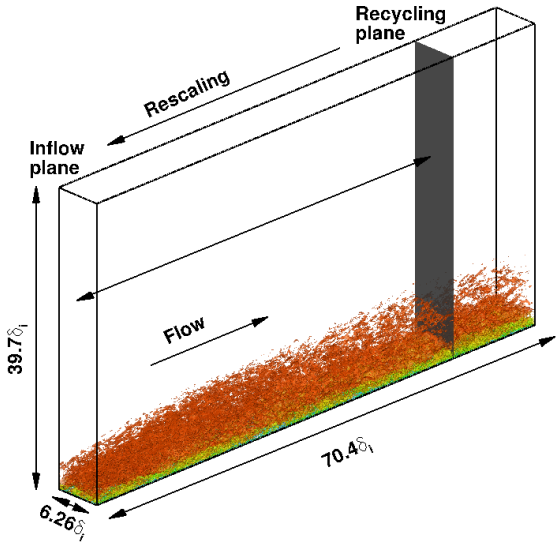

Figure 1. Computational domain and simulation setup for DNS of a Mach 6 turbulent boundary layer (Case M6Tw076).[14] The reference length δ_i is the thickness of the boundary layer (based on 99% of the freestream velocity) at the inlet plane. An instantaneous flow is shown in the domain, visualized by iso-surface of the magnitude of density gradient, $|\Delta\rho|\delta_i/\rho_\infty = 0.9825$, colored by the streamwise velocity component (with levels from 0 to U_∞, blue to red).

B. Baseline RANS of High-Speed Turbulent Boundary Layers

For RANS simulations of high-speed turbulent boundary layers, the Reynolds-averaged Navier Stokes equations are solved using ANSYS Fluent (V15.0)[15] with the shear-stress transport (SST) $k-\omega$ model of Menter.[16] The SST based $k-\omega$ model differs from the standard $k-\omega$ models in that it undergoes a gradual transition to the $k-\epsilon$ model in the outer part of the boundary layer. No low-Reynolds correction is used as the $k-\omega$ based model can be directly integrated from the wall.

Figure 2 shows a schematic of RANS computational domain under the condition of Case M6Tw076 along with the boundary conditions setup in the Fluent solver. Grid points of 561×150 are used in the streamwise and wall-normal directions. The streamwise and wall-normal domain sizes are approximately $L_x/\delta_r \times L_y/\delta_r = 180 \times 80$, respectively, where δ_r is approximately the boundary-layer thickness at the center of the domain. Uniform grids are used in the streamwise direction with a resolution of $\Delta x/\delta_r \approx 0.3$. Geometric grids with a stretching ratio of less than 1.05 are used in the wall-normal direction. The wall-normal grid resolution is $\Delta y^+ \approx 0.8$ at the wall and $\Delta y^+ \approx 20$ near the boundary-layer edge . Systematic grid refinement in each direction has been conducted to verify the grid convergence of the RANS results (Figure 3). The computational setup for RANS of other cases parallels that of the Case M6Tw076.

C. Physics-informed Machine Learning Approach

In this section, the physics-informed ML approach by Wang et al[9] is briefly summarized. The general idea of the ML approach is that given a set of training flows with data, the functional form of the discrepancy in the Reynolds stress modeled by RANS can be learned in the mean flow feature space. Based on the learned regression function of Reynolds stress discrepancy, a new flow with a different configuration or a different flow condition can be predicted. The mean flow features $\mathbf{q}$ as regression inputs are constructed by raw mean flow quantities such as pressure P, mean velocity U, fluid density ρ, and rate of strain tensor S. The complete list of mean flow features for incompressible flows can be found in Wang et al.[9,17] As the response of the regression, the discrepancy $\Delta\boldsymbol{\tau}$ of Reynolds stress is in its physical projections but not in its components. To obtain the physically meaningful projections of Reynolds stress, the following eigen-decomposition is performed:

$$\boldsymbol{\tau} = 2k\left(\frac{1}{3}\mathbf{I} + \mathbf{A}\right) = 2k\left(\frac{1}{3}\mathbf{I} + \mathbf{V}\Lambda\mathbf{V}^T\right). \tag{1}$$

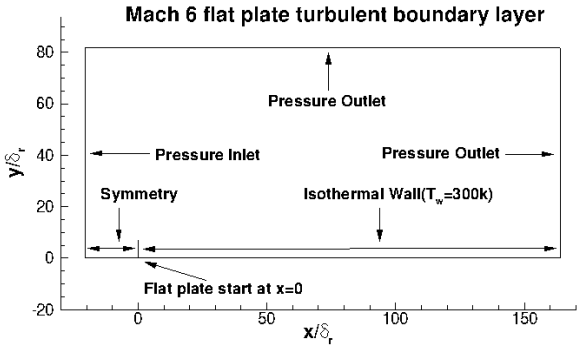

Figure 2. 2D computational setup and boundary conditions. δ_r is approximately the boundary-layer thickness at the center of the domain.

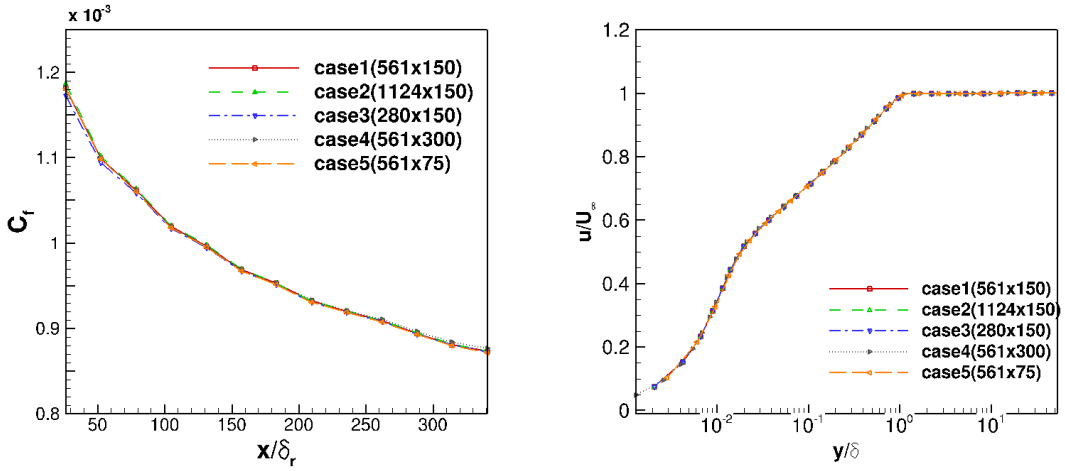

(a) (b)

Figure 3. Grid convergence study of RANS for Case M6Tw076.

The physical projections are magnitude k, shape Λ, and orientation $\mathbf{V}$ of Reynolds stress tensor.

The overview procedure is shown in Figure 4 and is summarized as follows:

1. Perform baseline RANS simulations on both the training flows and the test (prediction) flow.
2. Compute the fields of "feature" vectors $\mathbf{q}(x)$ (e.g., pressure gradient and streamline curvature, among others) based on the RANS predicted mean flow fields for each flow.
3. Compute the discrepancies field $\Delta\boldsymbol{\tau}(x)$ in the RANS modeled Reynolds stresses for the training flows based on the high-fidelity data.
4. Construct regression functions $\Delta\boldsymbol{\tau} = f(\mathbf{q})$ for the discrepancies based on the training data prepared in Step 3.
5. Compute the Reynolds stress discrepancies for the test (prediction) flow by evaluating the regression functions. The Reynolds stresses can subsequently be obtained by correcting the baseline RANS predictions with the evaluated discrepancies.

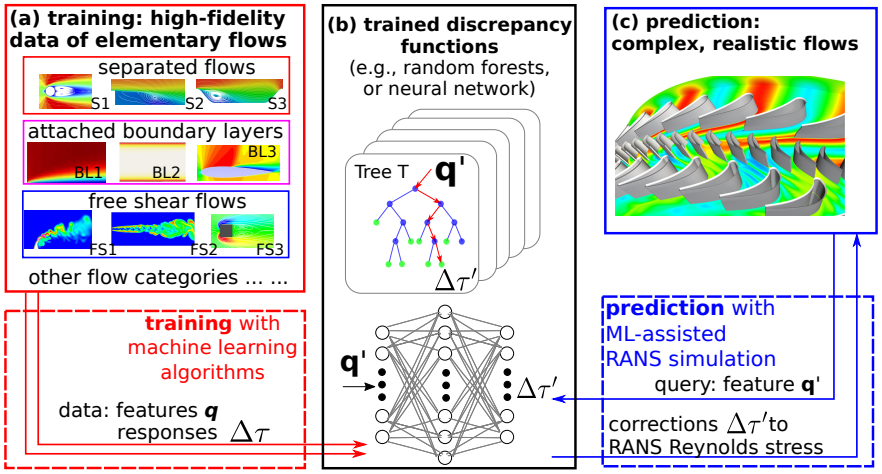

Figure 4. Overview of the Physics-Informed Machine Learning (ML) framework for predictive turbulence modeling. Data from training flows (panel a) are used to construct discrepancy functions of Reynolds stresses $\Delta\boldsymbol{\tau}(\mathbf{q})$ with respect to the mean flow features q by using machine learning algorithms (panel b). These functions are queried to provide Reynolds stress corrections in RANS simulations of complex flows (panel c). Panel (d) shows a feature space view of the training data provided by different classes of flows. Only two features (mean flow curvature and pressure gradient) are shown for illustration purposes.

The current study extends the aforementioned ML technique to high-speed boundary-layer flows. As an initial step towards the extension, we apply the machine-learning technique to high-Mach-number, zero-pressure-gradient, flat-plate turbulent boundary layers using the DNS database listed in Table 1. Table 3 lists the raw mean flow variable to construct the invariant basis used as the regression input vector $\mathbf{q}$ for learning the functional form of the discrepancy in RANS modeled Reynolds stress. The mean-flow features used in this particular study consist of only a subset of the full list given in Wang et al.,[9,17] and the temperature gradient ∇T is added to the incompressible-flow features in order to account for variations in thermodynamic quantities in compressible flows.

III. Results

In this study, we focus on demonstrating the physics-informed ML technique on cases where training and prediction flows have the same geometry of a flat plate (with different spatial domain sizes) but are different in flow conditions (e.g. the freestream Mach number M_∞ and the wall-to-recovery temperature ratio T_w/T_r). Table 4 summarizes the two machine-learning scenarios. In each scenario, we use the DNS data of a lower-Mach-number turbulent boundary layer as the training flow to build the random forest

Table 3. Raw mean flow features used as the regression input vector q to construct the invariant basis for learning the functional form of the discrepancy in RANS modeled Reynolds stress. The normalized feature $\hat{q}_i$ is obtained by normalizing each element of the corresponding raw input q_i with normalization factor q_i^* according to $\hat{q}_i = q_i/(|q_i| + |q_i^*|)$. Notations are as follows: U is mean velocity vector, k is turbulent kinetic energy (TKE), T is temperature, ρ is fluid density, ε is the turbulence dissipation rate, S is the strain rate tensor, C_p is the heat capacity at constant pressure, $\mathbf{\Omega}$ is the rotation rate tensor, $\|\cdot\|$ indicate matrix norm.

Normalized raw input $\hat{q}_i$	description	raw input q_i	normalization factor q_i^*
$\hat{\mathbf{S}}$	strain rate tensor	$\mathbf{S}$	$\frac{\varepsilon}{k}$
$\hat{\mathbf{\Omega}}$	rotation rate tensor	$\mathbf{\Omega}$	$\|\mathbf{\Omega}\|$
$\hat{\nabla k}$	gradient of TKE	∇k	$\frac{\varepsilon}{\sqrt{k}}$
$\hat{\nabla T}$	temperature gradient	∇T	$\|\mathbf{U}\cdot\nabla\mathbf{U}\|/C_p$

regressor. The random forest regressor thus built is in turn used to correct the RANS prediction of Reynolds stresses for a turbulent boundary layer at a higher Mach number (i.e. the prediction flow). The RANS results, after corrected by the ML technique, are tested and validated against DNS at the condition of the prediction flow.

Table 4. Summary of machine-learning scenarios.

Scenarios	Training flow	Prediction flow
SI	Case M25	Case M6Tw076
SII	Case M25	Case M8Tw053

In Scenario SI, Case M25 ($M_\infty = 2.5$, $T_w/T_r = 1.0$) is used as the training flow to correct the RANS results under the condition of Case M6Tw076 ($M_\infty = 5.86$, $T_w/T_r = 0.76$). Figure 5 shows a comparison of the Reynolds normal and shear stresses against DNS. The normal stresses ($\overline{\rho u_i' u_i'}$) corrected by ML have shown significant improvement over those of the baseline RANS. The improvement for the shear stress $\overline{\rho u' v'}$ is comparatively minor given that Menter's SST $k-\omega$ model used in the baseline RANS has already been well-tuned to give good predictions of the Reynolds shear stress for canonical flows like the attached flat-plate turbulent boundary layers at high speeds. Similar trend of the Reynolds-stress components is seen for Scenario S2 where the same DNS (i.e. Case M25) is used as the training flow to correct the RANS results under an even higher Mach number of Case M8Tw053 ($M_\infty = 7.87$, $T_w/T_r = 0.53$), as shown in Figure 6. Note that in this scenario, the training and prediction flows differ significantly in both the freestream Mach number and the wall-to-recovery temperature ratio.

Figures 7a and 7b show the turbulent kinetic energy (TKE) for Cases M6Tw076 and M8Tw053, respectively. Consistent with the Reynolds normal stresses, the TKE shows significantly better comparison with the DNS after corrected by ML.

To visualize the Reynolds-stress anisotropy, Figures 8 and 9 plot the Barycentric map at multiple streamwise locations for Scenarios SI and SII. The Reynolds-stress anisotropy shows significant improvement after corrected by the ML technique.

IV. Summary

In this paper, a physics-informed machine learning approach is applied to improve RANS modeled Reynolds stresses for high-speed flat-plate turbulent boundary layers using an existing DNS database. The effectiveness of the ML technique for improving Reynolds stresses is demonstrated on two scenarios where

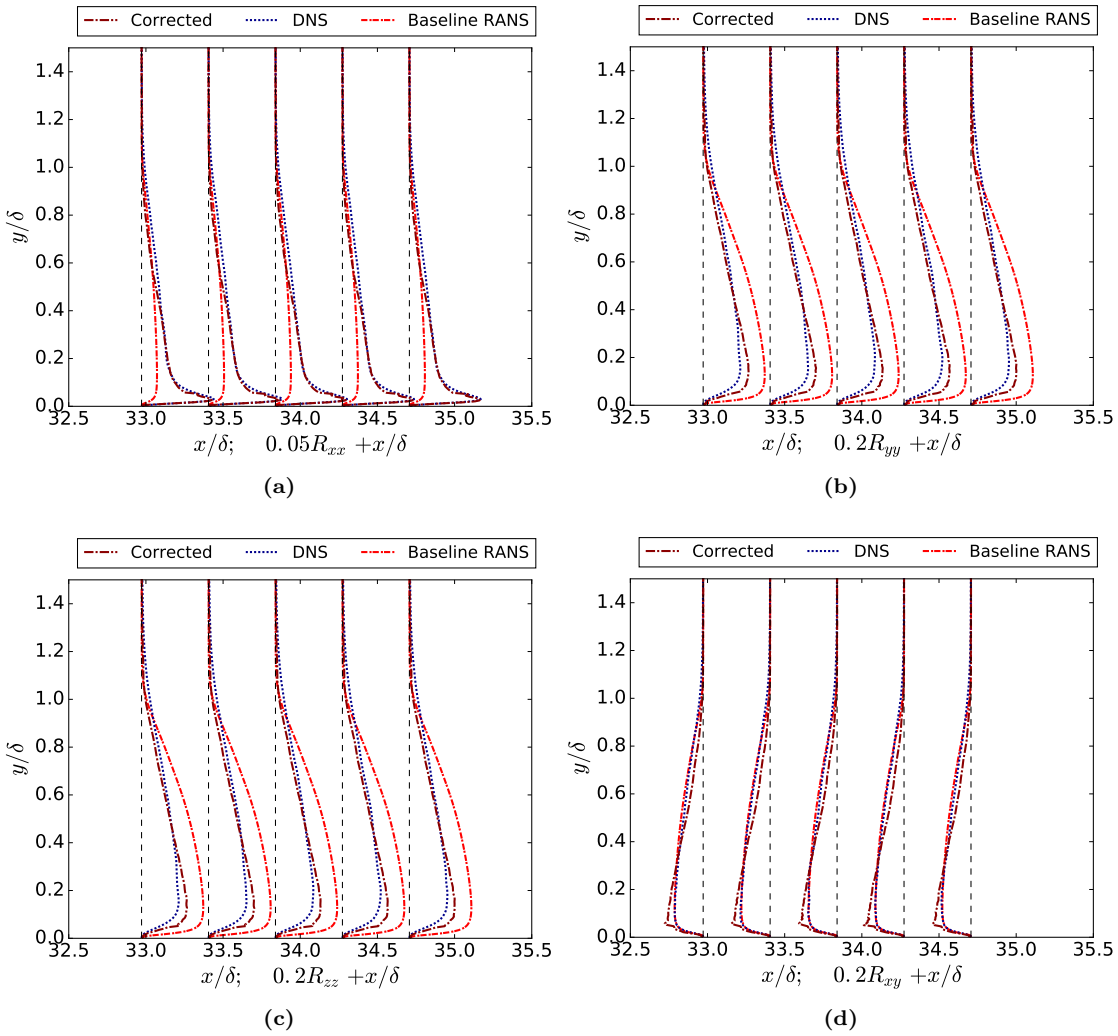

Figure 5. Comparison of RANS-predicted Reynolds stresses with the DNS for Case M6Tw076. (Scenario SI: Training flow: Case M25; Prediction flow: Case M6Tw076). (a) $\overline{\rho u'u'}/\tau_w$; (b) $\overline{\rho v'v'}/\tau_w$; (c) $\overline{\rho w'w'}/\tau_w$; (d) $\overline{\rho u'v'}/\tau_w$.

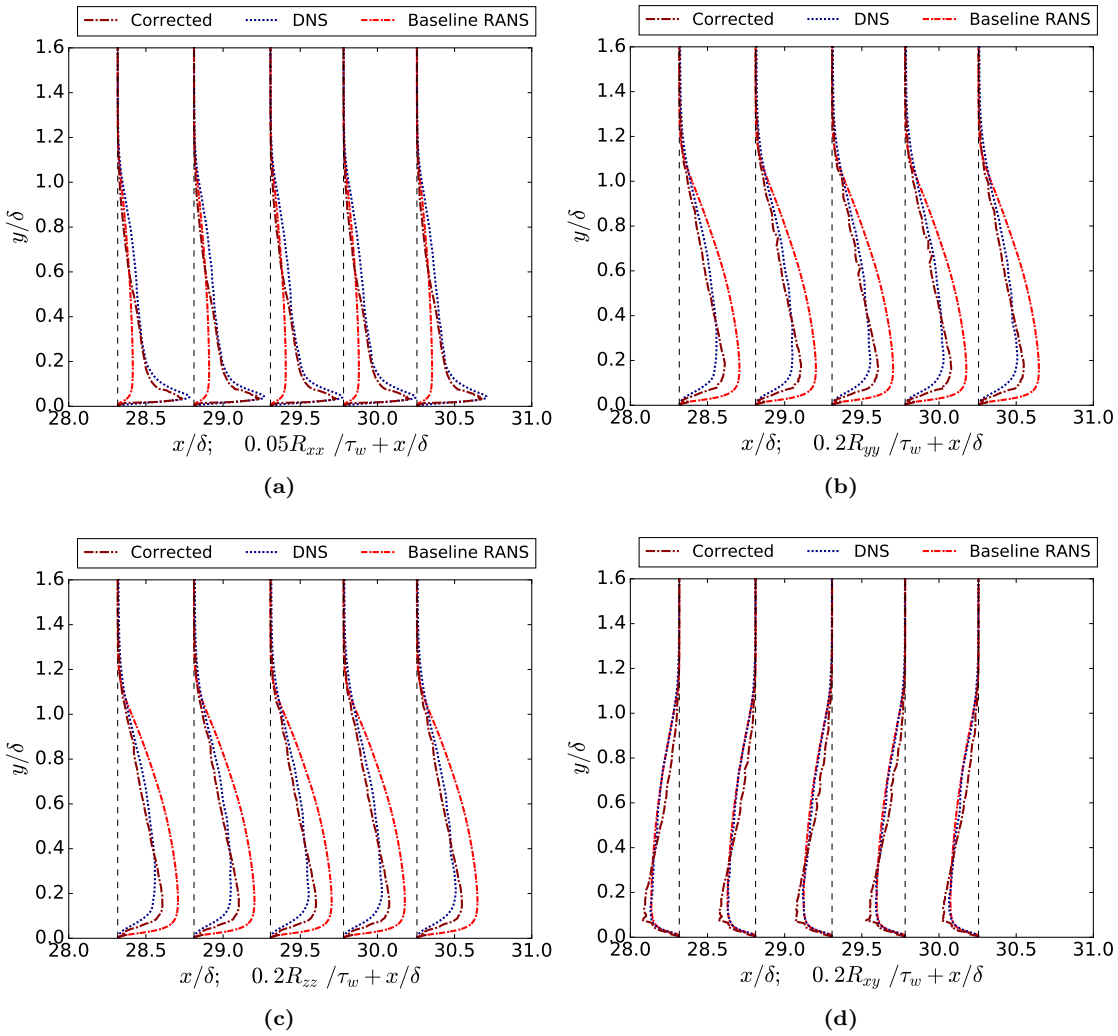

Figure 6. Comparison of RANS-predicted Reynolds stresses with the DNS for Case M8Tw053. (Scenario SII: Training flow: Case M25; Prediction flow: Case M8Tw053). (a) $\overline{\rho u'u'}/\tau_w$; (b) $\overline{\rho v'v'}/\tau_w$; (c) $\overline{\rho w'w'}/\tau_w$; (d) $\overline{\rho u'v'}/\tau_w$.

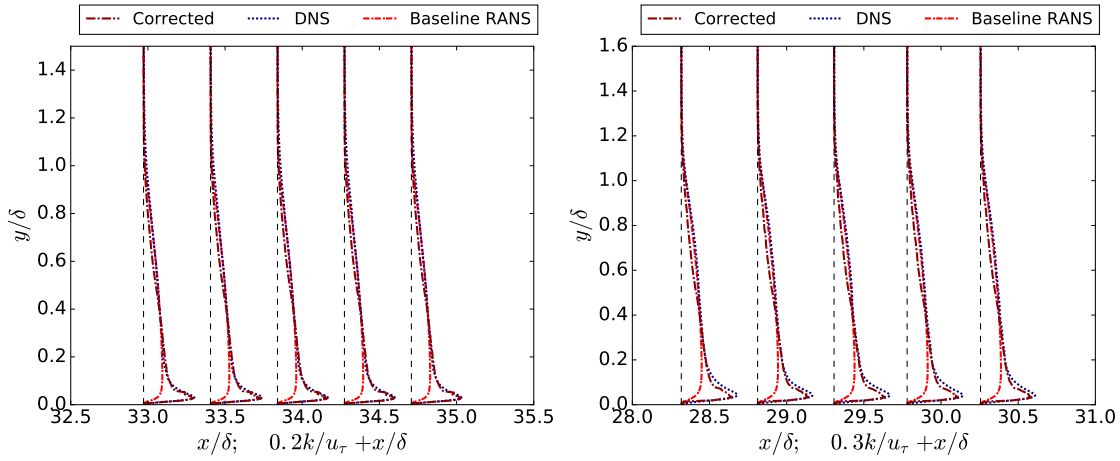

(a) Case M6Tw076 **(b) Case M8Tw053**

Figure 7. Comparison of RANS-predicted turbulent kinetic energy k/u_τ^2 with the DNS. (a) Case M6Tw076 (Scenario SI: Training flow: Case M25; Prediction flow: Case M6Tw076); (b) Case M8Tw053. (Scenario SII: Training flow: Case M25; Prediction flow: Case M8Tw053).

training and prediction flows have the same geometry of a flat plate but are different in the freestream Mach number M_∞ and the wall-to-recovery temperature ratio T_w/T_r. The study shows that the RANS predicted Reynolds normal stresses, the TKE, and the Reynolds-stress anisotropy of cold-wall hypersonic turbulent boundary layers (Case M6Tw076 and Case M8Tw053) can be significantly improved using the ML technique based upon a training flow of a supersonic boundary layer with an adiabatic wall (Case M25). Such a study lays the foundation toward better physics-based turbulence modeling for high-Mach-number turbulent flows.

Acknowledgments

The DNS database of high-speed turbulent boundary layers used in the paper is generated based on the work supported by the Air Force Office of Scientific Research under award number FA9550-14-1-0170, managed by Dr. Ivett Leyva. Computational resources for the DNS are provided by the DoD High Performance Computing Modernization Program and the NSF's Petascale Computing Resource Allocations Program (NSF ACI-1640865).

References

[1]Rumsey, C. L., "Compressibility Considerations for kw Turbulence Models in Hypersonic Boundary-Layer Applications," *Journal of Spacecraft and Rockets*, Vol. 47, No. 1, 2010, pp. 11–20.

[2]Wu, X., "Inflow Turbulence Generation Methods," *Annual Review of Fluid Mechanics*, Vol. 49, 2017, pp. 23–49.

[3]Smits, A. J. and Dussauge, J. P., *Turbulent Shear Layers in Supersonic Flow*, American Institute of Physics, 2nd ed., 2006.

[4]Oliver, T. and Moser, R., "Uncertainty quantification for RANS turbulence model predictions," *APS Division of Fluid Dynamics Meeting Abstracts*, Vol. 1, 2009.

[5]Dow, E. and Wang, Q., "Quantification of Structural Uncertainties in the k–ω Turbulence Model," *52nd AIAA/ASME/ASCE/AHS/ASC Structures, Structural Dynamics and Materials Conference*, AIAA, Denver, Colorado, 4-7 April 2011 2011, AIAA Paper, 2011-1762.

[6]Parish, E. J. and Duraisamy, K., "A paradigm for data-driven predictive modeling using field inversion and machine learning," *Journal of Computational Physics*, Vol. 305, 2016, pp. 758–774.

[7]Xiao, H., Wu, J.-L., Wang, J.-X., Sun, R., and Roy, C., "Quantifying and reducing model-form uncertainties in Reynolds-averaged Navier–Stokes simulations: A data-driven, physics-informed Bayesian approach," *Journal of Computational Physics*, Vol. 324, 2016, pp. 115–136.

[8]Ling, J. and Templeton, J., "Evaluation of machine learning algorithms for prediction of regions of high Reynolds averaged Navier Stokes uncertainty," *Physics of Fluids (1994-present)*, Vol. 27, No. 8, 2015, pp. 085103.

[9]Wang, J.-X., Wu, J.-L., and Xiao, H., "Using Data to Improve Reynolds Stresses in RANS Simulations: A Physics-Informed Machine Learning Approach," submitted, arXiv preprint arXiv:1606.07987.

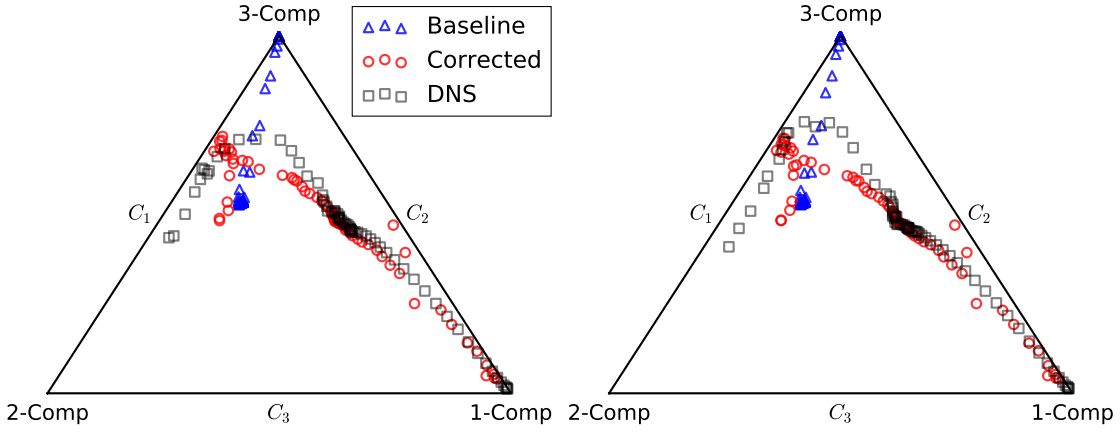

(a) $x/\delta = 32.97$ **(b)** $x/\delta = 33.41$

(c) $x/\delta = 33.84$ **(d)** $x/\delta = 34.27$

Figure 8. Barycentric map of the corrected Reynolds stress learned from flows for Scenario I (Training flow: Case M25; Prediction flow: Case M6Tw076). The corrected results (red circle) on four streamwise locations (i.e., $x/\delta = 32.97, 33.41, 33.84, 34.27$) are plotted in panels (a), (b), (c), and (d). Corresponding baseline results (blue triangle) and benchmark results (black square) are also plotted for comparison.

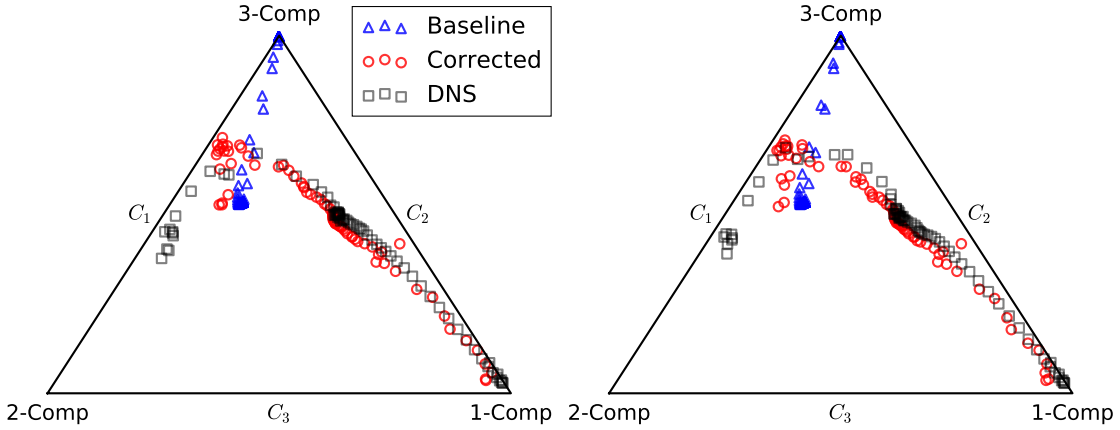

(a) $x/\delta = 28.32$ **(b)** $x/\delta = 29.13$

(c) $x/\delta = 29.94$ **(d)** $x/\delta = 30.74$

Figure 9. Barycentric map of the corrected Reynolds stress learned from flows for Scenario II (Training flow: Case M25; Prediction flow: Case M8Tw053). The corrected results (red circle) on four streamwise locations (i.e., $x/\delta = 28.32, 29.13, 29.94, 30.74$) are plotted in panels (a), (b), (c), and (d). Corresponding baseline results (blue triangle) and benchmark results (black square) are also plotted for comparison.

[10]Duan, L., Choudhari, M. M., and Wu, M., "Numerical Study of Pressure Fluctuations due to a Supersonic Turbulent Boundary Layer," *Journal of Fluid Mechanics*, Vol. 746, 2014, pp. 165–192.

[11]Duan, L., Choudhari, M. M., and Zhang, C., "Pressure Fluctuations induced by a Hypersonic Turbulent Boundary Layer," *Journal of Fluid Mechanics*, Vol. 804, 2016, pp. 578–607.

[12]Duan, L. and Choudhari, M. M., "Analysis of Numerical Simulation Database for Pressure Fluctuations Induced by High-Speed Turbulent Boundary Layers," *AIAA Paper 2014-2912*, 2014.

[13]Zhang, C., Duan, L., and Choudhari, M. M., "Acoustic Radiation from a Mach 14 Turbulent Boundary Layers," AIAA Paper 2016-0048, 2016.

[14]Duan, L. and Choudhari, M. M., "Numerical Study of Pressure Fluctuations due to a Mach 6 Turbulent Boundary Layer," *AIAA Paper 2013-0532*, 2013.

[15]"ANSYS Fluent User Guide, Release 15.0," *ANSYS Inc., November*, 2013.

[16]Menter, F. R., "Two-equation eddy-viscosity turbulence models for engineering applications," *AIAA journal*, Vol. 32, No. 8, 1994, pp. 1598–1605.

[17]Wang, J.-X., Wu, J. L., Ling, J., Iaccarino, G., and Xiao, H., "Towards a Complete Framework of Physics-Informed Machine Learning for Predictive Turbulence Modeling," Tech. rep., Proceedings of Summer Research Program, Center of Turbulence Research, Stanford University, Stanford, CA, USA, 2016.